Available online at www.sciencedirect.com
SCIENCE DIRECT®
Journal of Sound and Vibration 284 (2005) 421–453
JOURNAL OF SOUND AND VIBRATION
www.elsevier.com/locate/jsvi

Pulse–pressure loading effects on aviation and general engineering structures—review

J.R. Florek, H. Benaroya*

Department of Mechanical and Aerospace Engineering, School of Engineering, Rutgers, The State University of New Jersey, 98 Brett Road, Piscataway, NJ 08854, USA

Received 30 September 2003; accepted 18 June 2004
Available online 15 December 2004

Abstract

This paper reviews various aspects of modeling an explosion on an aircraft, which can be extended to more general structures. A brief summary of material and structural models is given, followed by a detailed history of pulse–pressure loading models with an emphasis on free–free beams and how pulse characteristics affect a structure's response. Techniques to desensitize pulse shape effects are discussed, which culminate in the form of pressure–impulse isodamage curves. Studies using random loading models are also presented.

1. Introduction

The designer must account for a variety of loadings which act on an aircraft during flight. These include, but are in no way limited to, lift, drag and weight of the structure, cargo, and passengers. But as a result of recent acts of terrorism, most notably the December 21, 1988 bombing of Pan Am Flight 103 over Lockerbie, Scotland [1] and the events of September 11, 2001, explosive loads, although grim, have also become a necessary consideration.

However, predicting the effects of an explosive load on a structure can be a difficult task. Due to the high number of uncertainties inherent to an explosion, two similar sources can produce two

*Corresponding author. Tel.: +1-732-445-4408; fax: +1-732-445-3124.
E-mail address: benaroya@rci.rutgers.edu (H. Benaroya).

0022-460X/$ - see front matter © 2004 Elsevier Ltd. All rights reserved.
doi:10.1016/j.jsv.2004.06.023

drastically different blasts with regard to total amount and range of damage. This point was illustrated by Gatto and Krznaric [2], who experimentally tested bomb explosions in luggage containers used in commercial airplanes. Using a charge detonated in the center of an empty container as a base line, they recorded substantial reductions in over-pressure when a similar charge was placed in a 50% or 75% full container. Furthermore, for a half-full container, the peak pressure value dropped nearly 97% when the bomb was moved from the top bag to three bags down inside the hold.

Moreover, depending on the nature of loading, a structure can exhibit both linearly elastic and nonlinearly plastic behavior on its way to failure. So both the load and structure must be modeled accurately to produce meaningful results. Chen [3] simulated the complex interaction between these two components for the specific case of an explosion on an aircraft. Here, the blast propagation was modeled as a fluid tetrahedral mesh, while the plane as a series of beam and shell elements. Meanwhile, Dietz [4] described a similar study which revealed that a relatively small increase in structural thickness resulted in a significant improvement in an aircraft's ability to withstand an internal explosion.

Keeping in mind this acute sensitivity between load and structure, the authors of this paper seek to present a review of work done to model pulse–pressure loadings and their effects on various structural models. As the amount of available literature regarding impact loading on elastic–plastic and plastic structures is quite large, an emphasis is placed on work that distinctly illustrates how altering attributes of the loading model changes the amount of deformation sustained by the structure. Techniques to eliminate response sensitivity to pulse shape are also covered. Additional focus is placed on studies regarding free–free beams, which best model an aircraft in flight, pressure–impulse isodamage curves, which serve as useful design tools, and probabilistic loading models, which more accurately depict bomb blasts than typical deterministic models.

2. Structural, material and loading models

Four geometric models are primarily used throughout the literature to represent a general structure. The most basic is a single degree of freedom (sdof) mass–damper–spring system. As detailed by Biggs [5], the sdof system, shown in Fig. 1(a), is governed by the simple equation

$$M\ddot{y} + C\dot{y} + Ky = P(t), \tag{1}$$

where y is the displacement of the lumped mass M, while C is the damping coefficient, K the structural stiffness, and $P(t)$ the equivalent applied pulse loading of the system. Also commonly used are a beam, a plate and a shell, all covered by Jones [6] and depicted in Figs. 1(b)–(d), respectively, with various boundary conditions. As already mentioned, recent finite element studies modeling aircraft response to bomb explosions have used beams and shells to represent the structure. However, analysis of both sdof systems and plates can also produce useful insight in terms of sensitivity to changes in both loading and aircraft structural model. Indeed, Fleisher [7] modeled the luggage container of Ref. [2] as a sdof mass–spring system, while Singh and Singh [8] used thin plates to represent aircraft skin panels.

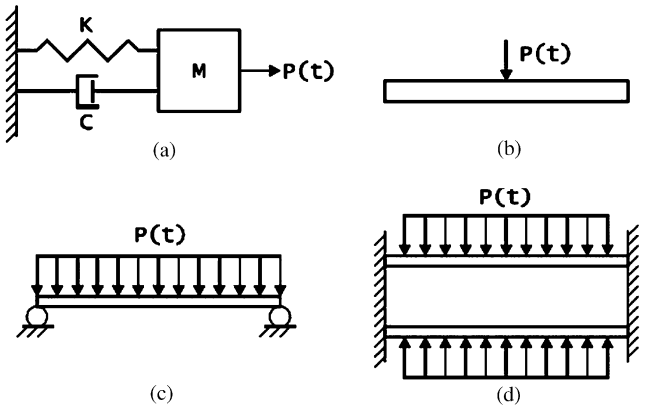

Fig. 1. Representative geometries with various boundary conditions and loadings: (a) a sdof model; (b) a free–free beam with a concentrated pulse load; (c) a simply supported plate loaded by a uniform pressure; (d) a clamped cylindrical shell loaded by a uniform pressure.

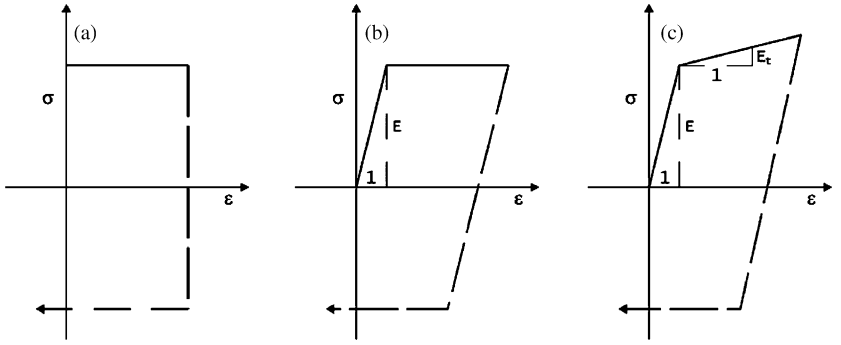

Fig. 2. Stress–strain diagram of (a) a rigid, perfectly plastic material, (b) an elastic, perfectly plastic material, and (c) an elastic–plastic hardening material, all with unloading.

The given geometries are varied with respect to not only boundary conditions, but also to material properties. Kaliszky [9] described five simple, applicable material models. By far, the most frequently encountered in the literature are a rigid, perfectly plastic and a linearly elastic, perfectly plastic material, whose stress–strain diagrams are shown in Figs. 2(a) and (b), respectively. Meanwhile, a linearly elastic material follows the form of a linearly elastic, perfectly plastic material, but only for stresses below the yield point. Also found are a rigid plastic hardening and a linearly elastic–plastic hardening material. These two models are identical to a rigid, perfectly plastic and a linearly elastic, perfectly plastic material, respectively, except that plastic deformation is now proportional to the load for stresses above yielding. The stress–strain diagram for the latter hardening material is shown in Fig. 2(c), where E_t is the tangent modulus.The applicability of a rigid, perfectly plastic material versus the more accurate, yet more complex, elastic–plastic model was discussed by Symonds [10]. Based on calculations for a sdof system subjected to an impulsive load, one where an infinitely large force acts over an infinitely

small time, Symonds stated that the relative error between the two models could be conservatively approximated by $1/R$, where R is the energy ratio between entirely plastic work and elastic strain energy capacity given by

$$R = \frac{Yu_f}{Yu_y/2} = \frac{2u_f}{u_y}, \tag{2}$$

where Y is the yield force, u_f is the final displacement of the sdof system, and u_y is the elastic displacement equal to Y/K, where K is the equivalent spring stiffness of the system. This criterion was shown to be valid only for very short pulse loadings, whose durations are much less than the system's natural period, $2\pi\sqrt{M/K}$.

Symonds also outlined some mode approximation techniques, which were presented in greater detail in Ref. [11], to estimate plastic deformation in more complicated structures. One such method was used by Schleyer and Hsu [12] to predict the response of an elastic–plastic beam subjected to a symmetrical pulse–pressure loading. As seen in Fig. 3, the beam was modeled in two nonrigid halves. The idealization shown in Fig. 2(b) was used to model the stress–strain interaction. Both nonlinear and rotational springs, with respective stiffness K_x and K_ϕ, acted at either beam end. The former modeled purely plastic behavior, while the latter elastic, perfectly plastic characteristics of variable support conditions and plastic hinges. A third rotational spring, one with the rigid, perfectly plastic characteristics of a central plastic hinge, connected the two beam halves. Strain rate and strain hardening effects were neglected. The calculated beam deflections were of the modal form:

$$w(x,t) = \sum_{i=1}^{n} \varphi_i(x) C_i(t), \tag{3}$$

where $\varphi_i(x)$ defines the cosinusoidal deformation mode shape and satisfies the geometric boundary conditions of a given structure, and $C_i(t)$ represents the generalized displacements that satisfy Lagrangian form equilibrium equations. The deflections passed through the following three stages:

I. The combination of elastic flexural and either elastic or plastic membrane deformations before the appearance of any plastic hinge.

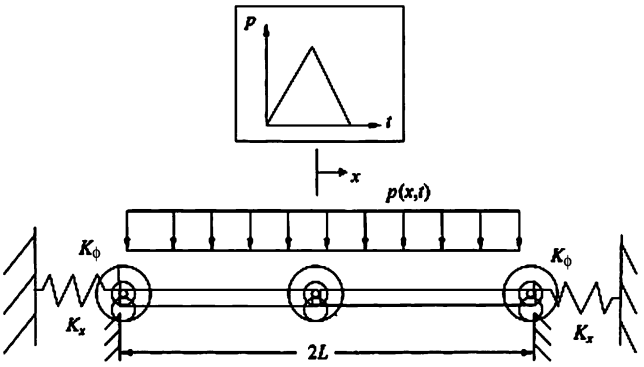

Fig. 3. Elastic–plastic beam model of Schleyer and Hsu [12].

II. The switch from purely elastic to elastic–plastic flexural deformations. Stage IIa corresponded to the switch when plastic hinges formed at the supports before the central moment reached the yield moment, stage IIb when the reverse occurred.
III. The switch to purely plastic flexural deformations, with plastic hinges formed at all three rotational springs.

These stages were processed numerically using a fourth-order Runge–Kutta time stepping scheme. Comparisons were made between the present model, an ABAQUS-generated finite element model, and various sdof models of other authors through plots of $w_{\max}/H$ versus p/p_c for various loading and boundary conditions. Here, H is the beam height, p the uniformly distributed pulse loading, and p_c the collapse load. Good agreement was found for cases of a rectangular and triangular pulse, shown in Fig. 4 along with other pulse shapes commonly used in the literature. The largest deviations occurred for small deflections in the elastic to elastic–plastic range for a beam with clamped ends. As the authors' technique is a modal approximation, accuracy can always be improved by increasing n in Eq. (3) for each stage definition.

The work of Schleyer and Hsu is representative of many papers found in the literature. Although the material and geometry assumptions may vary appreciably from one paper to the next, it is almost universal that maximum deflection is the key indicator of response. This deflection almost always occurs at the mid-point of a given geometry.

Further, the march through time while systematically checking critical values that define the onset of each deformation stage is also very common. Typical milestones include:

(1) The static collapse load being achieved at mid-span, which initiates the formation of a central plastic hinge. For a rigid plastic material, this event signifies the beginning of any deflection or

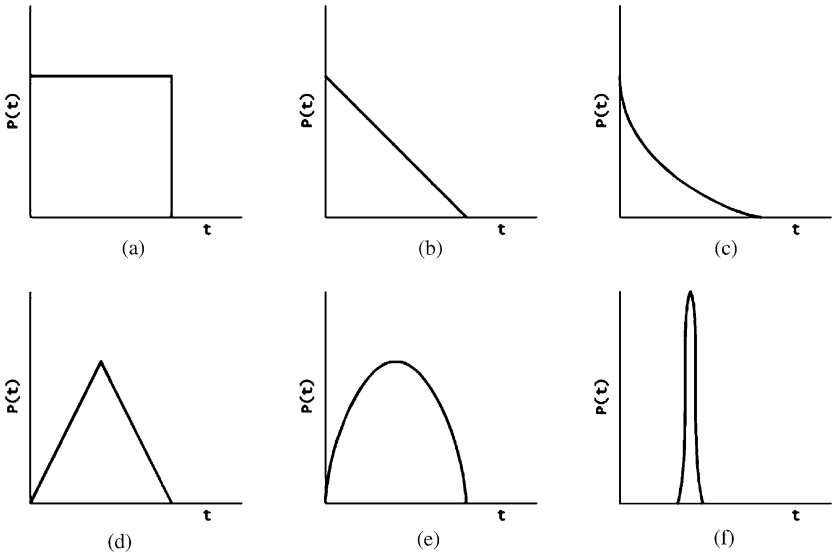

Fig. 4. Common pulse shapes: (a) rectangular; (b) linear decay; (c) exponential decay; (d) triangular; (e) sinusoidal; (f) impulsive load.

structural motion. When multiple effects are considered (e.g., shear and bending), a flow rule or yield condition usually defines this milestone.

(2) The formation of dual traveling plastic hinges symmetric to mid-span, if the centrally acting load is well in excess of the static collapse load. These hinges, which form in lieu of the single central plastic hinge, move toward one another with a continually applied load.

(3) The traveling plastic hinges reaching mid-span, subsequently disappearing.

(4) Bending forces becoming negligible after a critical deflection is achieved at mid-span (e.g., $H/2$ for a simply supported beam). At this point, only membrane forces act on the structure, which behaves as a string.

Numerous studies of the past thirty years using similar procedures have been briefed in a series of reviews by Jones [13–20]. These reviews covered a wide range of topics concerning the dynamic plastic behavior of structures including the effects of considering finite displacements, rotary inertia, strain hardening, strain rate sensitivity and transverse shear in the analysis. Unless otherwise noted, these specialized effects are assumed negligible throughout the remainder of this paper.

Further background can be found in Refs. [21,22]. The former text covers most of the topics presented in this section, as well as throughout this paper, focusing on the dynamic plastic behavior of cantilevers. Meanwhile, the latter text details explosive loads and their effect on engineering structures.

3. Pulse shape effects

An actual bomb explosion, like most blast loads, has a random pressure-time history. However, such an explosion invariably has a sharp pressure rise followed by a period of decay [22]. The pulse shapes shown in Fig. 4 serve as idealizations, which facilitate the analytical computation of structural response to such loads. They can easily be modified with respect to such attributes as total impulse, peak pressure achieved, rise time and pulse duration to best match an actual loading. It is clearly seen in Fig. 4 that only the triangular and sinusoidal pulses have finite rise times, while the other pulses all have instantaneous rises to a peak pressure. Furthermore, all of the pulses have gradual decays except for the rectangular and impulsive loads. It should be noted that all of these pulse shapes act over a very small period of time, usually only for a fraction of a second. The impulsive load is the limiting case which acts over zero time. Whereas the reviews by Jones [13–20] primarily covered the plastic response of fixed-ended beams, plates and shells to rectangular pulse loads, here, both plastic and elastic–plastic response of these structures and sdof models subjected to various pulse shapes are considered.

Hodge [23] compared deflection results attained for a circular cylindrical shell exposed to different shaped pulses having equal peak pressure and total impulse. He found that the deflection achieved by a square (rectangular in Fig. 4) pulse roughly approximated that by an exponentially decaying pulse only for pressures well in excess of the static collapse load, P_0. For loads with peaks less than $3P_0$, neither a square, trapezoidal nor doubly stepped pulse produced deflections within 18% of that rendered by the corresponding exponential pulse. Furthermore, Hodge showed that for such medium peaked loads having a finite rise time, a step could not be

substituted for a linear rise even though peak pressure and impulse would remain constant. Deviations between the two models increased substantially as peak pressure and rise time were increased. For the same load range, Hodge also compared the deflections achieved by square waves to that of a triangular pulse. With the same total impulse, the square wave results significantly overestimated that of the triangular wave. However, when only the impulses for pressures over P_0 were matched, the square underestimated the triangular results. This latter comparison of impulses is consistent with a rigid, perfectly plastic material assumption.

Using a simple constant-velocity recurrence formula to solve a nondimensional form of Eq. (1), Biggs [5] developed maximum response charts for an elastic–plastic sdof system subjected to a rectangular, linearly decaying, triangular and gradually applied load. For varying values of R_m/F_1, the ratio of yield load to maximum pulse load, the nondimensional maximum deflection, μ, was plotted versus t_d/T, the ratio of pulse duration to the system's natural period, for all four load shapes. The relationship between the time of peak response and the pulse duration, or where applicable rise time, was also charted. Meanwhile, Ayre [24] presented similar, but more extensive, ''response spectra'' for a wide variety of pulse shapes acting on undamped sdof systems. These shapes included various combinations of those depicted in Fig. 4. The charts of both Biggs [5] and Ayre [24] can serve as design tools as they clearly illustrate how altering certain pulse parameters (i.e., shape, pulse duration and rise time) affects the maximum deflection achieved by the sdof system.

Stronge [25] examined the effect of pulse shape on the deformation of a simply supported, rigid plastic beam subjected to a uniformly distributed pressure pulse. He sought to determine the pulse shape that would result in the maximum deflection when either the impulse or work done on the beam was constrained. In the former case, he found that the maximum possible deflection was produced by an impulsive load. In the latter, pulse shape was immaterial so long as the maximum pressure achieved was less than three times the static collapse load. This condition prevented the formation of dual symmetrical traveling plastic hinges which limit a beam's transverse deflection. These findings agreed with comparisons made to an exponentially decaying, a triangular and a doubly rectangular pulse, where the last pulse was simply the combination of two equal intensity rectangular pulses separated by a specified period of zero load.

Stronge [26] later presented a lower deflection bound for a variety of rigid plastic geometries subjected to both time and spatially varying loads. His work, along with the corresponding upper bound detailed by Robinson [27], is representative of all bounding theorems, which serve as common alternatives to analysis via modal approximation. The given bounds, based on an assumed, kinematically admissible velocity field, obviously bracketed the possible values of maximum deflection of a structure. For a simply supported beam acted on by a uniformly distributed pressure pulse, the lower bound solution for an exponentially decaying pressure pulse matched well with the exact rigid plastic solution. In contrast, bound solutions for rectangular and triangular (linearly decaying in Fig. 4) pulses severely underestimated response for maximum pressures up to twenty times the static collapse load. Furthermore, favorable comparisons were made between the present bound and others found in the literature for impulsively loaded fixed and cantilever beams, as well as for both simply supported and clamped circular plates and cylindrical shells subjected to rectangular pulse loads.

Symonds and Frye [28] compared the responses of sdof rigid plastic and elastic–plastic structures to low intensity pulse–pressure loading of varying rise time and duration. Continuing

the former author's earlier work [10], they dealt with rectangular, sinusoidal and linearly decaying pulses having peak values less than twice the static collapse load. For such loadings, they showed that a rigid plastic model was in good agreement with a corresponding elastic–plastic model when $\tau/T<0.1$ and $R>10$, where τ/T is the ratio of pulse duration to the system's natural period, and R is defined by Eq. (2). But for $\tau/T>0.1$, not only did errors between the models become large, they became nonconservative as well, underestimating the maximum displacement. Using the rectangular pulse as an example, -100% errors were found when $R=10$ at $\tau/T=0.9$ and when $R=50$ at $\tau/T=4$. Furthermore, Symonds and Frye observed that pulses with nonzero rise times yielded wavy curves when displacement was plotted versus τ/T for the elastic–plastic model. This behavior was contrary to analogous curves plotted for the rectangular and linearly decaying pulses not only in terms of smoothness, but also in that relative error tended to decay, albeit sinusoidally, for increasing pulse duration. Zero percent error was even achieved at regular intervals for sinusoidal and triangular pulses. The authors explained this tendency through comparison with dynamic amplification factors of elastic shock theory.

On a similar note, Zhang and Gross [29] remarked on the relationship between pulse shape and stress intensity factors in a cracked, infinite elastic solid. They showed that generally, dynamic overshoots of the stress intensity factor, $\bar{K}_I(t)$, were greatest early on (at times much less than the time it takes for a stress pulse to travel over a characteristic crack dimension) during the loading of an infinite pulse. Eventually, a static value of $\bar{K}_I(t)=1$ was reached. In contrast, for a finite pulse, stress intensity factor amplification increased with pulse duration, and statically $\bar{K}_I(t)=0$. Different peaks of $\bar{K}_I(t)$ were achieved for a step (rectangular in Fig. 4), linearly increasing, linearly decreasing, cosinusoidally decreasing, triangular, sinusoidal, trapezoidal and impulsive pulse.

Schubak et al. [30] proposed a simplified method for determining the response of a rigid plastic, doubly symmetric beam with fixed ends to distributed rectangular pulse loads of varying intensity. The authors decoupled the response into pure bending and pure string stages. Doing so enabled them to find, through study of triangular pulses, that rise time had little effect on the final maximum beam deflection, w_{0f}, for pulses having equal values of a nondimensional impulse parameter given by

$$\beta=\frac{p_m^2 t_p^2 N_0}{4mp_0 M_0}. \tag{4}$$

Here, p_m is the maximum pulse load achieved, t_p the pulse duration, m the beam mass per unit length, p_0 the static collapse load, and M_0 and N_0 are the respective fully plastic values of bending moment and axial load. Plots of $N_0 w_{0f}/M_0$ versus β for loads up to $10p_0$ showed a less than 10% difference between pulses with zero rise time and those that reached a peak at $0.3t_p$ for $\beta<1000$. For an infinite load, there was no difference at all.

Yankelevsky and Karinski [31] modeled a beam subjected to a symmetrical, distributed, short duration dynamic loading as two rigid half beams either simply supported or pin-hinged at the ends. Pulse loadings were either of rectangular, triangular (linearly decaying in Fig. 4) or exponential shape. The only deformation during loading occurred longitudinally in a finite number of elastic–plastic fibers, initially of zero length, which connected the two half beams. Unlike most of the models covered, the extension of the various fibers allowed for not only

calculation of a maximum deflection, but also of a time history of bending moments and membrane forces, as well as a stress and strain distribution. The nondimensional maximum deflection, $Y_{\max}/L$, of the beam compared well with the rigid plastic models of other works for each pulse shape, particularly at high pressures, where elastic effects became negligible and the fibers effectively served as a plastic hinge. For a triangular pulse with varying peak pressures, $Y_{\max}/L$ was plotted versus t_d/T, the ratio pulse duration to the beam's natural period. These plots showed that maximum deflection occurred at different pulse durations for each peak load case. Therefore, it seems that peak pressure has a greater influence on response than pulse duration for the considered loading values.

From this section, it is seen that:

- Pulse loading shape has a large effect on the deformation of various structural models. Some attributes of the loading seem to have a greater effect than others (e.g., peak pressure versus pulse duration).
- Plotting attributes of the loading against one another can be useful in the design process.
- A rigid plastic assumption is invalid for pressure intensities near the static collapse load and pulse durations near or above a structure's natural period. In these cases, elastic effects must be considered.

4. Free-free beams

In contrast to the studies of the previous section, those involving free-ended beams are now discussed. With no end constraints, the free–free beam more accurately represents an aircraft in flight. Papers on the dynamic loading of free–free beams date back over fifty years. However, in the last twenty years, an emphasis has been placed on how energy is dissipated in such a beam.

In an early study, Lee and Symonds [32] analyzed the deformation of a rigid, plastic free–free beam subjected to a triangular point pulse at mid-span. As a means of quantifying when one of the milestones listed in Section 2 was reached, a dimensionless loading parameter was defined as

$$\mu = \frac{Pl}{M_0}, \tag{5}$$

where P is the point load at a given time, M_0 is the limit moment, and l the half-length of the beam. Milestone (1) was reached when $\mu = 4$, milestone (2) when $\mu = 22.9$. Unlike in most papers, the deformation was not measured in terms of deflection, but rather in terms of a deflection angle, θ_0. This angle was plotted as a function of time for different values of pulse duration, $2T$, and μ_m, given by Eq. (5) when P is maximum. The time at which θ_0 achieved a maximum, and the beam a steady-state response, was shown to be roughly $0.3\mu_m T$. The rigid plastic assumption used was deemed applicable when:

$$\frac{\theta_0}{M_0 T^2/ml^3} \gg \frac{\tau^2}{2.5T^2},$$

where m is the beam mass per unit length, and τ is the beam's fundamental period of elastic vibration.

Symonds [33] reported on the same model subjected to rectangular, sinusoidal and triangular point pulses at mid-beam. For all three load shapes, he plotted the theoretical maximum deflection angle, θ_{0m}, as a function of μ_m. By doing so, Symonds found an empirical relationship between the maximum deflection angle and some of the load characteristics given by

$$\theta_{0m} = \frac{A}{mM_0^{5/3}l^{1/3}} I^2 P_m^{2/3}, \tag{6}$$

where I is the impulse, and P_m the maximum pressure of a particular loading. The constant A depended on load shape, taking on values of 0.043, 0.037 and 0.031 for a rectangular, sinusoidal and triangular pulse, respectively. Eq. (6) was found to be reasonably valid for $15 \leqslant \mu_m \leqslant 50$. However, Hodge [23] showed that this equation cannot be extended to other geometries, particularly to a circular cylindrical shell.

Jones and Wierzbicki [34] analyzed the response of a uniform, rigid plastic free–free beam subjected to a triangularly distributed, rectangular pressure pulse. They found that as the load became impulsive, only 25% of the input energy went into plastically deforming the beam. The remaining 75% caused a rigid body acceleration. The authors also briefed on the response of a nonuniform stepped beam subjected to a uniformly distributed pressure. They considered these two particular cases to ensure the onset of plastic deformation, as a free–free beam only moves as a rigid body if it is both uniform and subjected to a similarly uniform pressure pulse. In addition, a simple model of an aerospace vehicle was developed using a free–free stiffened cylindrical shell. Assuming failure due to tensile rupture, they obtained the following relationship between pulse duration time, τ, and pressure magnitude, p_0:

$$\tau = \sqrt{\frac{C\varepsilon_c}{p_0(\eta - 1)}}, \tag{7}$$

where ε_c is the critical failure strain, η is the ratio of p_0 to the collapse load, and C accounts for the shell's geometry. Eq. (7) was used to generate failure envelopes, which illustrate what combination of η and τ will cause rupture failure. Some such envelopes are given in Fig. 5. The authors noted that plastic rupture is not necessarily the cause of failure in all shells. Failure could also occur due to plastic crumpling, plastic tearing or elastic fracture, none of which were considered in the present study.

Yu et al. [35] considered an elastic–plastic free–free beam subjected to either a projectile impact at mid-span or a triangularly distributed impulsive load. Their analysis assumed small deflections and allowed for rotary inertial effects. A straightforward finite difference scheme was used to calculate the transverse deflection w, acceleration $\ddot{w}$, curvature κ, and bending moment M along the entire beam for a given time interval. For the case of projectile impact, bending moment was plotted versus position at twenty different time instances from 0.048 to 3.321 ms after impact. As such, it was shown that the impact-induced flexural waves travel through four phases. Phase 1 described the formation of the elastic–plastic wave and its motion towards the free end. The motion of the point of maximum bending moment was related to that of a traveling plastic hinge. Phase 2 and 3 entailed the first and second respective appearance of the hinge moving back and forth. In these stages, the wave that reflected off the free end interfered with the hinge. Finally, in phase 4, the traveling hinge vanished as the beam rotated about mid-span, much like a stationary

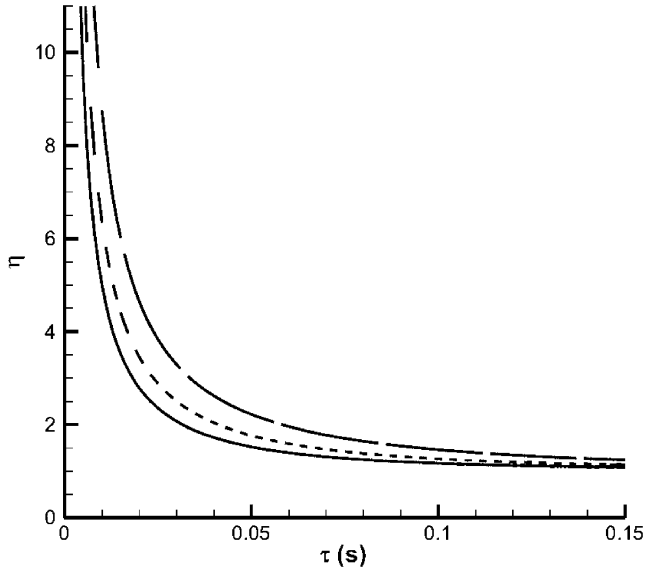

Fig. 5. Failure envelopes of a simplified aerospace vehicle for various critical strains, when $C = 0.03986$: ——, $\varepsilon_c = 5\%$; – – –, $\varepsilon_c = 8.5\%$; — —, $\varepsilon_c = 17\%$.

plastic hinge. Smith and Hetherington [22] provided an introduction on stress wave propagation, while Smart [1] detailed the potential devastating effects that such wave propagation, as induced by a bomb blast, can have on an aircraft.

Moreover, Yu et al. [35] compared the behavior of their elastic–plastic model with that of a rigid plastic simplification through use of conservation of energy and an energy ratio, R. Their R was similar to the one of Eq. (2) with the initial kinetic energy of the impact mass substituted for plastic work capacity in the numerator. In terms of the total input energy, 38% was dissipated plastically as $R \to \infty$, while 21% was dissipated plastically and 17% elastically when $R = 2$. In both cases, the remaining 62% of input energy was converted into the kinetic energy which caused rigid body motion of the beam. On a deflection basis, the rigid plastic model matched well with the elastic–plastic model, particularly at the beam's mid-span. Both models captured the general trend of an experimentally tested beam.

For the case of the triangularly distributed load, Yu et al. [35] illustrated that 75% of input energy was converted to rigid body kinetic energy. Obviously, a rigid plastic model predicted the remaining 25% went into plastic work. However, an elastic–plastic model predicted substantial elastic work at low R values, dependent on the slenderness ratio of the beam, L/h. As L/h decreased, so too did the amount of energy going into elastic work. Therefore, the rigid plastic model, which is a minimum bound for elastic effects, becomes more applicable with shorter free–free beams. Furthermore, a corresponding maximum bound was given in the form of a simplified elastic–plastic model. This model assumed that two rigid plastic beam halves were connected by an elastic–plastic rotational spring, similar to the beam in Fig. 3. The error analysis used by Yu et al. [35] to compare elastic–plastic and rigid plastic results mirrors that used in Refs. [10,28].

Yang and Xi [36] compared the theoretical deformation of a free–free beam found from a linearly elastic–plastic hardening model with experimental results. Their small deflection model included rotary inertial terms. Derived from a minimum energy principle and in keeping with the elastic–plastic hardening model of Fig. 2(c), their finite difference scheme was more complicated than that used by Yu et al. [35]. In addition to the four quantities found by Yu et al., Yang and Xi's scheme calculated the axial displacement u, axial acceleration $\ddot{u}$, stress σ, strain ε, axial force N, and second-order moment L along the entire beam for a given time interval. Moreover, three coefficients of the governing equation, A, B and C, also needed to be evaluated at every iteration. For an impact acting transversely at a quarter-point of the beam, six stages of motion were observed. Four of these corresponded to the phases noted by Yu et al. for an impact acting at mid-span. The first additional stage covered the time between one wave first reflecting off the short end and its opposite wave's first reflection off the long end. The other stage described the period that followed the end of rotation about a stationary hinge at the point of impact. In this final stage, the beam moved as a rigid body as it vibrated purely elastically. However, the beam was found to dissipate less plastic work when loaded at a quarter-point than at mid-span. Therefore, failure due to plastic damage is more likely to occur when a beam is loaded symmetrically as opposed to unsymmetrically. The theoretical and experimentally observed motions again agreed with one another.

Yang et al. [37] examined the small deflection response of a rigid, perfectly plastic free–free beam subjected to a concentrated step (rectangular in Fig. 4) load. Unlike in most studies, they not only varied the magnitude of the load, P, but also the position along the beam where it acted. As a result, the authors discovered five different response mechanisms. These are shown in Fig. 6, where L is the beam half-length, M_p the fully plastic bending moment, and β a measure of position. Mode I was a rigid body motion, while modes II and III were both single hinge mechanisms. Meanwhile, mode IV developed a double hinge and mode V a triple hinge. The beam was found to be most resistant to deformation when the load was applied at a critical value of $\beta = 0.6595L$. This is the value where the first four response modes intersect one another in Fig. 6. In contrast, the beam was found to be least resistant to damage when the load was applied to the free end ($\beta = 1$). Here, the beam finished the rigid body mode at the smallest possible P. Furthermore, as in Refs. [34,35], the partitioning of input energy was examined. Rigid body motion was found to consume at least 67% of the available energy, which could be higher depending on the response mechanism. This value was slightly higher than the 62% noted by Yu et al. [35] for a projectile impact at the beam's mid-span. As a rigid plastic assumption was used, no energy went into elastic deformation.

Ahmed et al. [38] studied a finite element elastic–plastic free–free beam model subjected to either a single or two point impact load. Each load was delivered by an independent impactor. Newmark's time integration scheme was used to solve the coupled nonlinear system, which was strain rate sensitive and governed by a von Mises yield criterion. Their approach compared well with that of Yu et al. [35] and a rigid plastic assumption for a single point impact at mid-span. In contrast though to previous studies, the impactor was allowed to separate completely from the beam during rigid body motion. After separating early on, the impactor and beam eventually rejoined. However, the splitting resulted in only about 21% of the initial impactor kinetic energy being eventually transferred to the beam, over half of which resulted in rigid body motion. For

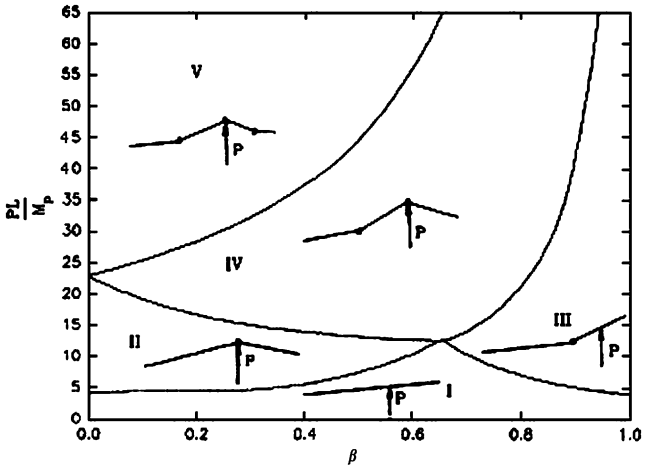

Fig. 6. Response modes for a free–free beam for varying load magnitudes and positions [37].

the two point load case, about 37% of the initial energy transferred to the beam. Again, just over half of this total went into rigid body motion, the rest into deforming the beam.

Other studies involved the response of damaged free–free beams. Zhang and Yang [39], as well as Ruan and Yu [40], examined the effect a small notch in the beam had on how the beam deformed and dissipated energy. These beams were shown to go through the same deformation modes illustrated in Fig. 6, and dissipate energy similarly to the beams in previously discussed studies, except when the loading occurred near the notch. This work can be extended to show how initially small damage sustained by an aircraft can eventually result in failure.

From this section, it is seen that:

- Concerns with regard to pulse shape and a rigid plastic assumption for previously discussed geometries extend to free–free, and particularly slender, beams.
- The majority of energy input on a free–free beam goes into rigid body motion, not plastic deformation.
- Failure envelopes can serve as useful design tools, depicting the combination of loading parameters that result in structural failure.
- Where a free–free beam is impacted can affect what deformation mode it adheres to, how energy is dissipated and how flexural waves propagate through the beam.

5. Eliminating pulse shape effects

For over thirty years, Youngdahl [41] has worked on the problem of eliminating pulse shape effects on the response of various structures. Early on, he examined rigid, perfectly plastic models of a circular plate, reinforced circular cylindrical shell, free–free beam and circular shell. The first two were subjected to uniform pressure, the third to a concentrated force at mid-span, and the last to a ring load. The pulse shapes, which constituted each of these loadings, were taken as

rectangular, linearly decaying, exponentially decaying, triangular and sinusoidal. For each of the four structural models, Youngdahl sought to unify the maximum deflection achieved by each of the five pulse shapes. In doing so, he determined key parameters of a pulse which, when equal for dissimilar shapes, would predict approximately equal deflections. The first of these parameters was the total impulse defined by

$$I_e = \int_{t_y}^{t_f} P(t)\,\mathrm{d}t, \tag{8}$$

where $P(t)$ is the loading function and t_y and t_f are the times when plastic deformation begins and ends, respectively. The second was the effective load defined by

$$P_e = \frac{I_e}{2t_{\mathrm{mean}}}, \tag{9}$$

where t_{mean}, the time interval between the onset of plastic deformation and when the centroid of the pulse occurs, is given by

$$t_{\mathrm{mean}} = \frac{1}{I_e}\int_{t_y}^{t_f} (t - t_y)P(t)\,\mathrm{d}t. \tag{10}$$

For a rectangular pulse with constant pressure P and pulse duration τ, $I_e = P\tau$, $t_{\mathrm{mean}} = \tau/2$ and therefore, $P_e = P$. So the definition for effective load, given by Eq. (9), simply reduces an arbitrarily shaped pulse into an equivalent rectangular pulse of equal impulse.

For the first three structure types, the maximum deflection, $W_0(t_f)$, was found to be equal to $I_e^2 f(P_e)$, where $f(P_e)$ is a derived function, different for each structure type. This relation was only approximately true for the circular shell, whose governing equations were more awkward to evaluate. As such, when $W_0 P_y/I_e^2$ was plotted versus P_e/P_y for each pulse shape of a particular structure, where P_y is the static yield pressure, the five resultant curves were nearly indistinguishable. The largest deviation occurred, as expected, with the approximated circular shell solution. In contrast, the plotted shape curves were clearly differentiable when the abscissa P_e/P_y was replaced by $P_{\max}/P_y$. Fig. 7(a) shows this differentiability for the specific case of a free–free beam, where γ is the beam mass per unit length, and L the beam half-length. Meanwhile, Fig. 7(b) shows how all curves nearly collapse onto the rectangular curve of Fig. 7(a) when $W_0 P_y/I_e^2$ is plotted versus P_e/P_y. Youngdahl's method virtually eliminated load shape effect altogether from the response of the four given structures. This result is important since precise measurement, as well as prediction, of an entire pulse shape and peak force value can prove to be difficult.

When the pulse–pressure loading is not uniform, P becomes a function of both position and time. For a rigid, perfectly plastic circular cylindrical shell, Youngdahl [42] took $P(z,t)$ as the product of a load shape $\Phi(z)$, purely dependent on axial position, and a pulse shape $\Psi(t)$, purely dependent on time and analogous to the pulse shapes of Fig. 4. In order to reduce both load and pulse shapes to equivalent rectangles as he did for $P(t)$ in his earlier paper, Youngdahl defined an effective load and effective pulse shape. The former was defined as

$$\Phi_e = \frac{[\int_0^{z_y} \Phi(z)\,\mathrm{d}z]^2}{2\int_0^{z_y} z\Phi(z)\,\mathrm{d}z},$$

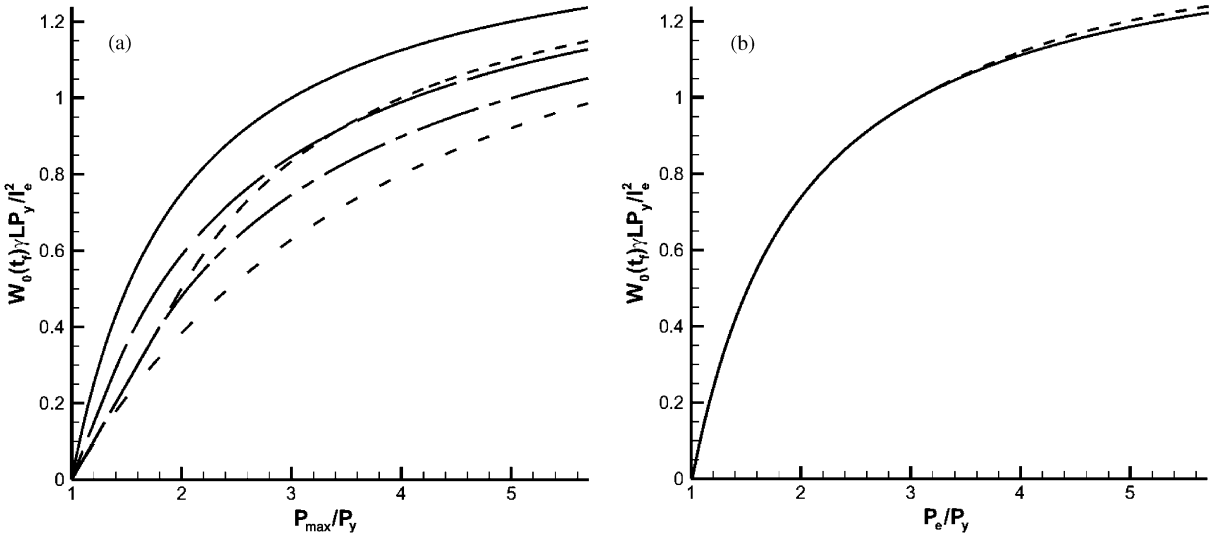

Fig. 7. Dependence of $W_0(t_f)P_y/I_e^2$ for a free–free beam on (a) $P_{\max}$: ——, rectangular; – – –, linear decay; — —, sinusoidal; — – —, triangular; – –, exponential decay; (b) P_e: ——, rectangular, linear decay; – – –, exponential decay, sinusoidal, triangular pulse.

where z_y is the initial location of a formed plastic hinge. Meanwhile, the effective pulse shape, Ψ_e, was given by Eq. (9), substituting $\Psi(t)$ for $P(t)$. As a result, various load shapes collapsed onto nearly a single curve when $U_0\rho P_0 RH/I_e^2$ was plotted versus $L_e/\sqrt{RH}$. Here, U_0 is the maximum deflection, ρ the surface density, P_0 a function of P_y, R the radius, H the thickness, and L_e is the effective half length of the loaded region given by

$$L_e = \frac{1}{\Phi_e}\int_0^L \Phi(z)\,\mathrm{d}z,$$

where L is the actual half length of said region. Furthermore, the plots of $U_0\rho P_0 RH/I_e^2$ versus Ψ_e for a rectangular, triangular and exponentially decaying pulse were also virtually identical. Therefore, response of a cylindrical shell can be made independent of both load and pulse shape. Should this result be extended to more general structures, the modeling of a space- and time-dependent explosive load can be made significantly easier.

However, should L be a function of time, the analysis of a rigid plastic shell becomes considerably more difficult. Youngdahl [43] found that for such a case the final deformation depended on four parameters. The effective applied force, F_e, was analogous to that defined in Eq. (9), while the effective applied moment, G_e, was defined by substituting the applied moment $G(t)$ for $P(t)$ in Eqs. (8)–(10). Further, the final deformation also depended on the effective half-length L_e, now a function of the impulses of both applied load and moment, and the deflection attained if the load was purely impulsive. These parameters were also significant in Youngdahl and Krajcinovic's treatment [44] of an infinite plate subjected to a general pressure pulse. Moreover, additional complications arose in the shell analysis if the now time-dependent L was

growing. These included an increased pulse shape effect on response and an inapplicability of standard modal techniques.

Youngdahl [45,46] applied similar techniques to a simply supported rigid, plastic circular plate. His earlier work assumed a uniform pressure distribution, while the later, an axisymmetric, but otherwise arbitrary distribution. Unlike in Ref. [42], Youngdahl [46] determined that the pressure $P(r,t)$ acting on a circular plate did not need to be represented as the product of a load and a pulse shape. For loads below that which would cause the formation of a central hinge band, maximum deflection was found to be a function of only P_e and t_{mean}, defined in Eqs. (9) and (10), respectively. However, for higher loads, maximum deflection was found by

$$W(0,t_f) = f(P_e, t_{\text{mean}}) - f(P_e^*, t_{\text{mean}}^*),$$

where f is the same function that defined maximum deflection at lower loads, and P_e^* and t_{mean}^* have identical formulations to that of P_e and t_{mean} except that the bounds of integration t_y and t_f are now the time instants when the hinge band forms and vanish, respectively. This subtraction principle held despite the problem being nonlinear in nature.

Furthermore, Youngdahl [47] considered the effect of rigid plastic strain hardening on a sdof system. He calculated the maximum deflection of the system, $U(\omega,t_f)$, in terms of three parameters. The first two, I^* and F_e^*, were analogous to I_e and P_e, defined in Eqs. (8) and (9), respectively. The third, which characterized the effect of strain hardening, was given by

$$\Omega^* = \frac{\omega I^*}{F_y}, \tag{11}$$

where ω is the natural frequency of the system, and F_y is the yield load. However, unlike in the previous studies, these parameters could not be associated with an equivalent rectangular pulse. In order to do so, thereby making the parameters more physically meaningful, the stars were simply dropped from these definitions. In other words, three alternative parameters were defined, where I was given by Eq. (8), F_e by Eq. (9), and Ω by Eq. (11) with I^* replaced by I. Plotting $U(\omega,t_f)F_y/I^2$ versus F_e/F_y for various values of Ω, curves for a rectangular, exponentially decaying and ramped pulse collapsed onto one another only when $\Omega<1$. As Ω increased, the curves noticeably separated, but nonetheless kept the same general shape while remaining relatively close to one another. By allowing $t_f \to \infty$ in the definitions of I, F_e and Ω, three additional parameters, I_0, F_{e0} and Ω_0, were also defined. These new parameters, which were more easily calculated, made the total impulse and effective load independent of ω. However, when $U(\omega,t_f)F_y/I_0^2$ was plotted versus F_{e0}/F_y, the three pulse shape curves diverged even more and no longer maintained the same trend when $\Omega>\pi$. This divergence was partly attributed to the need for higher order moments, usually associated with stochastically loaded models, when calculating $U(\omega,t_f)$ for an increasing Ω. Not withstanding, eliminating pulse shape effects is considerably more difficult when strain hardening is taken into account.

From this section, it is seen that:

- The pulse shape effect can be virtually eliminated for many rigid plastic geometries subjected to a uniform loading.

- Structures with nonuniform loading distributions can also be dealt with, but require more complicated integral expressions in the calculation of effective parameters.
- Considering specialized effects, such as strain hardening, further complicates these calculations.

6. Pressure–impulse isodamage curves

As noted by Abrahamson and Lindberg [48], pressure–impulse characterization schemes have been in use for nearly fifty years. Such a scheme, shown in Fig. 8, serves as a simple design tool that clearly illustrates what combination of pressure and impulse of a given load will produce an equal structural response. When a response, predicated by maximum deflection, is deemed critical, pressure–impulse pairs that fall above and to the right of the corresponding curve are deemed unsatisfactory. Such pairs will result in structural failure. In contrast, pairs that fall below and to the left of the critical curve are viewed as acceptable.

Abrahamson and Lindberg developed pressure–impulse ($P-I$) curves for rectangular, triangular (linearly decaying in Fig. 4) and exponentially decaying loads acting on a variety of structures. These structures included linear elastic and rigid plastic sdof spring–mass systems, as well as rigid plastic beams and plates. As seen in Fig. 8 for the linear spring–mass system, the curves for the three different pulse shapes only collapsed onto one another for values of P/P_0 or I/I_0 greater than 10, where P_0 is the magnitude of the step load, and I_0 the ideal impulse that individually produces a critical displacement. The deviations at mid-curve were about 20% for the sinusoidal and triangular load, and about 40% for the sinusoidal and conservative rectangular load. Similar discrepancies arose with the other geometries, which indicate that pulse shape is universally important in determining a structure's critical response. In spite of this finding, the hyperbolic $P-I$ curve shape, with asymptotes at both P/P_0 and $I/I_0=1$, was consistent for all pulse shapes. This general shape established three load regions—the short-duration region

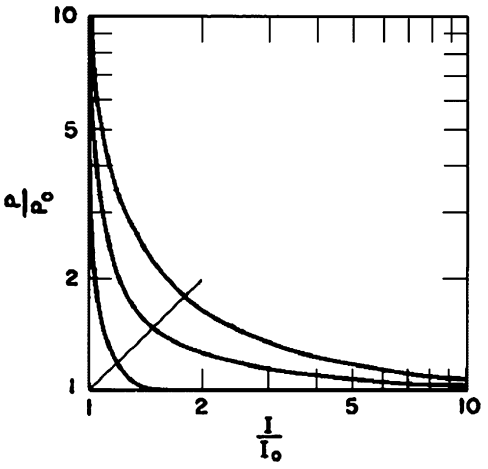

Fig. 8. Critical load curves for a linear spring–mass system: rectangular, triangular, exponential load from left to right [48].

controlled by impulse, the long-duration region controlled by maximum pressure, and the mid-duration region mutually controlled by both pressure and impulse. The curve shape also suggested an approximation of the form:

$$\left[\frac{P}{P_0}-1\right]\left[\frac{I}{I_0}-1\right]=1.$$

This equation best matched the $P-I$ curves of the exponentially decaying loading function for both sdof models. Furthermore, the authors found that for this pulse shape, with the form: $P(t)=P_{\max}\exp(-t/T)$, a critical displacement was most efficiently achieved when the decay constant $T=\tau/4$, where τ is the system's natural period. They also suggested a means of deriving a critical curve for more complex structures. This method entailed breaking the structure into simpler parts, superposing each part's $P-I$ curve onto a single plane, and taking the most conservative outline.

Zhu et al. [49] used Youngdahl's work [41] to develop characteristic curves (c.c.) for rigid, perfectly plastic models of a simply supported beam and circular plate, as well as a reinforced circular cylindrical shell, subjected to a uniformly distributed pulse loading. These curves illustrated what combination of total impulse and effective load, given by Eqs. (8) and (9), respectively, would lead to structural failure according to the Tresca yield criterion. I_e/I_0 was plotted versus P_e/P_y for each of the first five pulse shapes in Fig. 4 acting on a given structure, where I_0 is the ideal impulse. Just as in Youngdahl's work, the five resultant curves were nearly indistinguishable. Moreover, the c.c. of the different geometries were also nearly identical. This result implies that such curves may be independent of structural geometry. As such, the authors proposed that for an arbitrary pulse shape and geometry, the c.c. can be given by

$$\frac{6}{5}\left(\frac{I_e}{I_0}\right)^2\left(1-\frac{P_y}{P_e}\right)=1 \quad \text{when } \frac{P_e}{P_y}\leqslant 2, \tag{12}$$

$$\left(\frac{I_e}{I_0}\right)^2\left(1-\frac{4P_y}{5P_e}\right)=1 \quad \text{when } \frac{P_e}{P_y}\geqslant 2. \tag{13}$$

Zhu et al. [49] also sought to simplify the calculation of the total impulse, I_e. For nonrectangular pulses, the time when plastic deformation ends, t_f, must be found iteratively from a zero velocity condition given by Ref. [41] as

$$P_y(t_f-t_y)=\int_{t_y}^{t_f}P(t)\,\mathrm{d}t. \tag{14}$$

Once t_f is found, I_e is given by either side of Eq. (14). To eliminate the need for iteration, Zhu et al. defined the impulse, I, and effective load, P'_e, as in Eqs. (8) and (9), respectively, except that t_y was now taken as zero, and t_f as the time when the pulse loading is removed ($t=\infty$). When I/I_0 was plotted versus P'_e/P_y, the five resultant c.c. for each of the three geometries clearly deviated from one another for $P'_e/P_y<2$. Consequently, when using the simplified impulse and effective load, Eq. (12) becomes invalid.

Vaziri et al. [50] produced what they termed "isoresponse curves", which served the same purpose as the characteristic curves of Abrahamson and Lindberg [48] and Zhu et al. [49]. Their research was exclusive to a rigid, perfectly plastic beam with either simply supported or clamped

end conditions subjected to a rectangular pulse. The beam deflected according to the milestones of Section 2 and the simple flow rule given by

$$\frac{M}{M_0} + \left(\frac{N}{N_0}\right)^2 = 1,$$

where M is the bending moment, N the axial load at the beam's mid-span, and M_0 and N_0 are the respective fully plastic values of these quantities. They plotted isoresponse curves, namely P_m/P_0, the ratio of pulse intensity to collapse load, versus β from Eq. (4), for small and large deflections (low and severe damage), as measured by the deflection ratio δ_f/h, of beams with both end conditions. In each case, the clamped end curves were slightly to the right of their simply supported equivalents. Even though Vaziri et al. plotted pressure as a function of the impulse squared ($p_m^2 t_p^2$ of Eq. (4) reduces to I^2 for a rectangular pulse), these curves, shown in Fig. 9, appear similar to the $P-I$ curves in Fig. 8, with three clearly distinguishable load regions. Furthermore, the curves also resemble the failure envelopes for a free–free beam, shown in Fig. 5. In terms of range of applicability, Vaziri et al. stressed that even for small deflections, geometry changes have a significant effect on the beam's dynamic behavior. They also predicted that their rigid plastic model would be nonconservative for low intensity pulses loaded for a length of time approximately equal to the beam material's elastic period. This prediction was confirmed by Symonds and Frye [28].

In two papers, Li and Meng [51,52] extended Youngdahl's work to eliminate pulse load shape effects in both sdof elastic and elastic–plastic structures. Solving Eq. (1) for zero initial displacement and velocity and no damping, a nondimensional pressure and impulse were

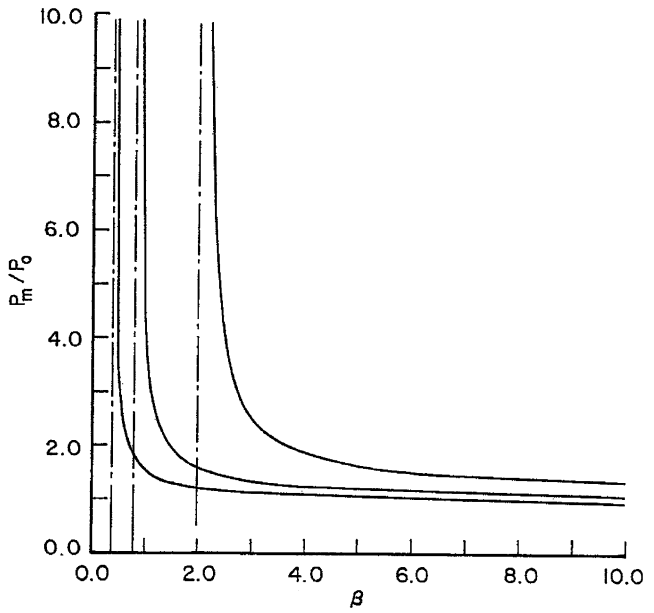

Fig. 9. Isodamage curves for low damage of a clamped beam: $\delta_f/h = 0.25, 0.5, 1.0$ from left to right [50].

obtained, given by

$$p = \frac{F_m}{y_c K} = \frac{1}{\int_0^{\tau_m} f(\tau') \sin(\tau_m - \tau') \, d\tau'} \tag{15}$$

and

$$i = \frac{I}{y_c \sqrt{MK}} = p \int_0^{\tau_d} f(\tau) \, d\tau, \tag{16}$$

where F_m is the maximum value of the load $F(t)$, $f = F/F_m$, y_c is a pre-defined critical displacement, and τ_m and τ_d are nondimensional values of maximum deflection and loading times, respectively. From the nondimensional pressure and impulse, isodamage curves, also referred to as pressure–impulse ($p - i$) diagrams, were generated. Just as Abrahamson and Lindberg [48] had done, Li and Meng [51] broke the $p - i$ diagram into three distinct regimes. Again, the first was controlled by the impulse, while the last, the quasi-static regime, by the pressure. Both p and i contributed in the dynamic regime II where the curve satisfied

$$g(p, i) = \frac{y_{\max}}{y_c} = 1, \tag{17}$$

where $g(p, i)$ is a parabolic shape function, and $y_{\max}$ the maximum structural displacement achieved for a given loading. A structure fails when $g(p, i) > 1$. It should be noted that the $p - i$ diagram actually follows Eq. (17) throughout all regimes, with impulse driving the equation in regime I and pressure in regime III. However, like in Ref. [48], it was only in regime II that the isodamage curves for a rectangular, triangular (linearly decaying in Fig. 4) and exponentially decaying pulse differed from one another. To eliminate the shape effect in this regime, Li and Meng proposed an empirical method. The pair defined the effective pressure and impulse as

$$p_e = \frac{1}{i_e} + 0.5 \tag{18}$$

and

$$i_e = \frac{(i - 1)^{n_2}}{n_1}, \tag{19}$$

where n_1 and n_2 are solutions of two different least squares-derived quadratic equations involving a particular pulse shape's centroid. Values of n_1 and n_2 for the three pulse shapes mentioned are given in Table 1. This least squares approximation to eliminate shape effect does not seem as satisfying as the derived method of Youngdahl [41]. As the quadratic approximating equation was based on only the centroids of the three given pulse shapes, there is no guarantee that a fourth pulse shape's values of n_1 and n_2 will continue their trend. Further, the $p_e - i_e$ diagrams for the three given pulse shapes, although closer together than their respective $p - i$ diagrams, were not at all collapsed onto a single curve. Then again, the assumption of an elastic material prevented the same mathematical simplifications that Youngdahl used for a rigid plastic material from being applied here.

For a sdof elastic–plastic structure, Li and Meng [52] used the material model illustrated in Fig. 2(b). As such, the response followed a more general case of Eq. (1), where K was replaced by a defined resistance function $R(y)$, whose value at yielding is R_0. The resultant $p - i$ diagram

Table 1
Sample n values for various pulse shapes for use in Eq. (19)

	Rectangular	Triangular	Exponential
n_1	0.035	0.150	0.300
n_2	0.850	0.700	0.700

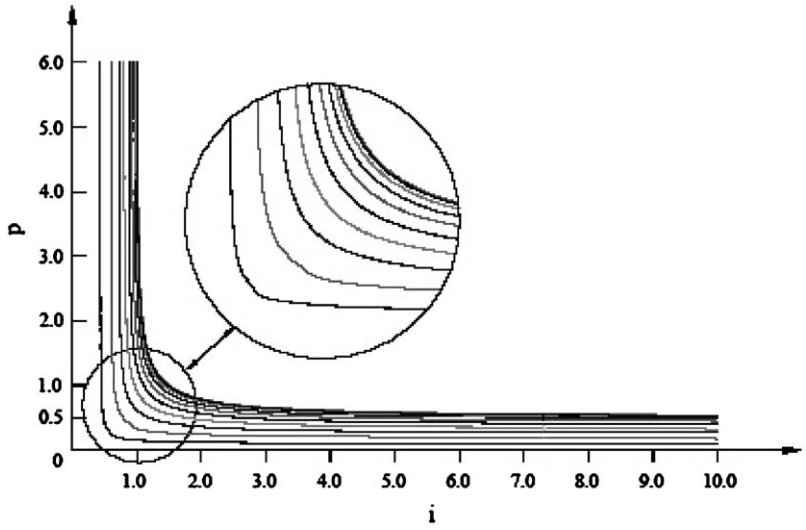

Fig. 10. $p-i$ diagram for an exponentially decaying load acting on a sdof elastic–plastic system: $\alpha = 0.1, 0.2, 0.3, 0.4, 0.5, 0.6, 0.7, 0.8, 0.9, 1.0$ from left to right [52].

followed Eq. (17) just like the elastic case considered earlier, where p and i are defined as in Eq. (15), save the third term, and Eq. (16). Also as before, the authors recognized that their resultant $p-i$ curve, shown in Fig. 10, was influenced by loading pulse shape. To remove this influence, they suggested using the empirical method of their earlier work, given by Eqs. (18) and (19). Li and Meng claimed that the $p-i$ curve for the elastic–plastic structure was also influenced by a parameter α defined as

$$\alpha = \frac{R_0}{y_c K}. \tag{20}$$

To remove the curve's influence on α, the authors suggested transforming p and i to $p/h_1(\alpha)$ and $i/h_2(\alpha)$, respectively, before satisfying Eq. (17), where $h_1(\alpha)$ and $h_2(\alpha)$ are least squares, quadratic functions of α. This procedure seems rather arbitrary. First, the end result was a single $p-i$ curve for each load shape, instead of the ten shown in Fig. 10. Each single curve appeared to be almost identical to that of its corresponding nontransformed case for $\alpha = 0.8$. Moreover, for a

given material, the quantity R_0/K represents the elastic yield deflection, which is a constant. Therefore, by Eq. (20), only the assigned critical deflection y_c will vary α. Since y_c defines the $p-i$ diagram by Eq. (17), α should inherently influence the isodamage curve, shifting it just as the deflection ratio, δ_f/h, did the isoresponse curve for Vaziri et al. [50].

Li and Meng [52] also derived an expression for the $p-i$ diagram of a sdof rigid plastic structure. Using nondimensional versions of the impulse and pressure of Eqs. (8) and (9), called i_e and p_e, respectively, the following relation held:

$$\frac{y_f}{y_c} = \frac{i_e^2}{2}\left(\frac{1}{\alpha} - \frac{1}{p_e}\right), \tag{21}$$

where y_f is the final and maximum deflection achieved, and α is still given by Eq. (20). The expression for the resultant isodamage curve was found by setting Eq. (21) equal to 1 as per Eq. (17). The $p-i$ diagram of the sdof rigid plastic structure had the same general shape as that of the purely elastic and elastic–plastic sdof cases. Li and Meng noted that Eq. (21) agreed with Youngdahl's assertion that maximum deflection for a general rigid, plastic structure is of the form $I_e^2 f(P_e)$.

Li and Jones [53] studied the dynamic response of a fully clamped, rigid plastic circular plate subjected to a uniform general blast loading. They accounted for both bending and shearing effects. The deformation mode was found to depend on a dimensionless parameter given by

$$v = \frac{Q_0 R}{2M_0}, \tag{22}$$

where R is the radius of the plate, and Q_0 and M_0 are, respectively, the transverse shear force and bending moment per unit length required for plastic flow. For different values of v, the dimensionless mid-point deflection, $\overline{W}_0$, was plotted versus a modified P_e of Eq. (9) for a rectangular, linearly decaying and exponentially decaying pressure loading. The modification to P_e was the same as made by Zhu et al. [49] in defining P'_e. The plots showed that values for the three pulse shapes collapsed onto a single curve for $v \leqslant 3$, and nearly onto a single curve for higher values of v. Therefore, the method of Youngdahl [41] to eliminate pulse shape effects is applicable even when transverse shear forces are considered. Li and Jones further modified the effective impulse and pressure of Youngdahl [41] by substituting t_1, the response time of the transverse shear sliding phase, for t_f in Eqs. (8) and (9). The resulting I_1 and P_1 were used to develop critical curves for mode III failure, when transverse shear severs around the supports, of a fully clamped circular plate. These curves, shown in Fig. 11, followed the form of Eq. (21) with i_e and p_e, respectively, replaced by nondimensional versions of I_1 and P_1, and α substituted with a function of v. Note that for larger values of v, the $i_1 - p_1$ curves deviate from the distinct three-regime curves of Refs.[48,50–52], which neglect shear effects.

Li and Jones [54] used a similar approach when dealing with a rigid plastic, short cylindrical shell acted on by a blast loading. But in this case, boundary conditions were taken as either simply supported or fully clamped, depending on the value of a parameter k, while the circumferential membrane force was considered in addition to the respective longitudinal bending and transverse

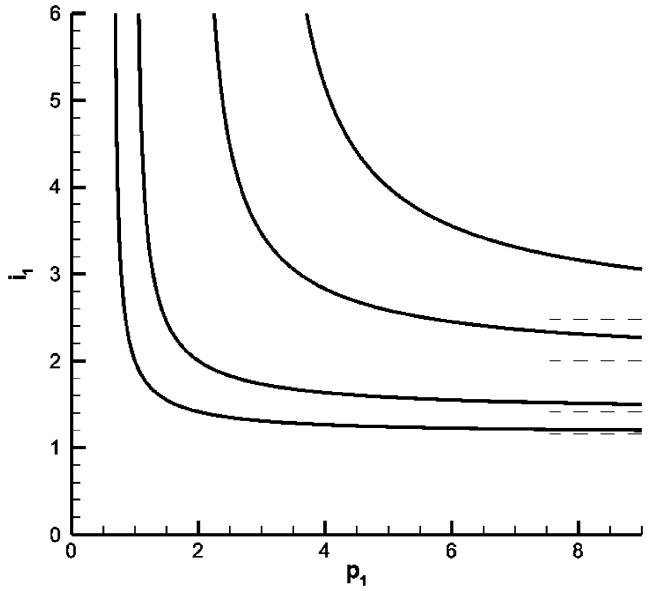

Fig. 11. Critical curves for severance around the supports of a fully clamped circular plate: $v = 2$, 3, 4, 5 from left to right. Dashed lines represent case as $p_1 \to \infty$.

shear forces. Furthermore, the shell deformation mode depended on two other parameters. The first was a modified v of Eq. (22), where the shell half-length L was substituted for R. The second was a parameter c, defined by

$$c^2 = \frac{N_0 L^2}{2M_0 R}, \tag{23}$$

where R is the radius of the shell and N_0 the membrane force per unit length required for plastic flow. For a fully clamped shell ($k = 1$), $\overline{W}_0$ was again plotted versus the modified P_e for the three different load shapes, but this time for different values of both c and v. The pulse shape curves again virtually collapsed onto one another, though deviations were more noticeable for the lower c value cases. In general, shear forces were found to most likely cause failure for high intensity loads acting on a fully restrained shell with low values of both c and v. Yet, shear effects were found to have less of an influence on a cylindrical shell than on either a rigid plastic plate or beam, as discussed in Ref. [55].

From this section, it is seen that:

- P–I diagrams all have the same parabolic shape with three distinct regions of response.
- The P–I diagram of a complicated structure can be derived from the diagrams of simpler, constituent pieces.
- Methods discussed earlier to eliminate pulse shape effect can be used to compare P–I diagrams of different geometries.
- The parameters of Eqs. (22) and (23) can be used to determine if considering shear effects is necessary.

7. Other sensitivities to loading models

In general, making small changes to the loading model should only cause small changes to a structure's response. However, as documented in numerous studies, sometimes small perturbations of the load can produce radically different deflection values in terms of both magnitude and direction. Examples of such behavior are now discussed.

Santiago and Bhattacharya [56] analyzed the sensitivity of a plate's response to loading details via computer simulations of a bomb blast. Six finite element models were used for the plate. The elastic, elastoplastic and combined (material and geometric) nonlinear models, each with either fixed or sliding edges, which served to bracket the actual boundary conditions of an experimental setup, were subjected to three different loadings. Although these loadings differed significantly in terms of shape, maximum pressure achieved and total impulse, they were based on the same explosion model, but calculated via hydrocode using different spatial intervals. As the mesh became finer, peak values of pressure and impulse increased. Response was found to be predominantly influenced by the impulse intensity, which is not surprising since the loading time was taken as approximately one-ninth of the plate material's natural period for all trials. Hence, the maximum deflection should occur in the short-duration region of the isodamage curve, which according to Abrahamson and Lindberg [48] is controlled by impulse. The two edge conditions produced no visible effects in the elastic and elastoplastic materials, while for the combined nonlinear model, the maximum deflection was moderately higher in the sliding end case of all three load runs. Generally, the maximum deflections were found in the elastoplastic models, the lowest in the most accurate combined nonlinear model. Meanwhile, for all loading trials, the elastic models exhibited a complete recovery and reversal of deflection direction. For some trials, the combined nonlinear model exhibited a similar, but much less drastic reversal of deflection.

For the past two decades, Symonds and various workers have examined structures that similarly deflect in a counterintuitive manner, in a direction opposite that of the applied load, for a small range of forcing values. Symonds and Yu [57] first noted such behavior while using the finite element code ABAQUS to perform analysis on a pin-ended, elastic–plastic beam subjected to a uniformly distributed rectangular pressure pulse. They compared their displacement results with those furnished by colleagues using seven other codes for the same problem. None of the results matched each other, and many exhibited the counterintuitive behavior. Attempting to analytically explain this behavior, the authors made use of a simpler Shanley-type elastic–plastic model subjected to a point load at mid-span. This model was identical to the one used by Yankelevsky and Karinski [31], except that there were only two elastic–plastic fibers in the cell connecting the two rigid half beams. For this model, Symonds and Yu found that a key parameter was ϕ_0, the beam angle when pulse unloading began. When ϕ_0 was greater than the angle at which fully plastic tension begins, the model deflected in the expected direction. In contrast, when ϕ_0 was less than the fully plastic angle, the model could deflect in the opposite direction. The authors surmised that if the structure was only loaded partly into the plastic phase, it would exhibit much less resistance to snapping back than the fully plastic structure. In their example, counterintuitive deflection occurred only when ϕ_0 fell between 0.086 and 0.092 rad. This range was represented by a slot in a characteristic diagram plotting extreme rotation angles versus ϕ_0.

Borino et al. [58] continued this work, attempting to explain the anomalous behavior of a damped Shanley-type model in terms of the system's total and elastic strain energy. By plotting these energies as a function of beam rotation angle for various values of ϕ_0, they were able to visualize and interpret the complicated behavior. Whereas the undamped case of Symonds and Yu [57] yielded one slot in the characteristic diagram, the lightly damped trial ($\zeta = 0.1$) of Borino et al. produced two smaller slots in the same vicinity. However, with arbitrarily small damping ($\zeta = 0.01$), 25 such slots appeared in the range $0.071 < \phi_0 < 0.098$ rad. Therefore, the undamped system is not a limiting case of the very lightly damped system. Moreover, it cannot even correctly predict the direction of the final displacement of its damped counterpart. Damping was noted to have two consequences. It reduced the total energy, bringing the system to equilibrium, and changed the shape of the final elastic strain energy curve, making it more difficult for the counterintuitive behavior to occur. As their energy analysis only involved the beam's recovery history following the first displacement maximum, the exact shape of the applied pulse was immaterial.

Lee et al. [59] extended research on the subject to a fixed-ended, two degree of freedom (2dof) Shanley-type model with additional elastic–plastic cells at the quarter points. Meanwhile, Qian and Symonds [60] analyzed the pin-ended, elastic–plastic beam with which Symonds and Yu [57] first observed the counterintuitive phenomenon. These models showed a much greater sensitivity to both the amount of damping and magnitude of the point load, P, than the previously discussed sdof model. This acute load sensitivity is clearly seen in Fig. 12 for $\zeta = 0.01$. In both studies, the energy approach of Borino et al. [58] was used, power density spectra were plotted and the Lyapunov characteristic exponent (LCE) calculated for various loads to interpret this chaotic behavior. Power density spectra, covered in Section 8, depict chaotic behavior in terms of energy spikes at certain key frequencies, while the LCE does so quantitatively. But unlike Lee et al., Qian and Symonds used Galerkin's method, which assumes deflections of the modal form of Eq. (3), to derive the equations of motion. This method furnished simpler equations to solve at each iteration.

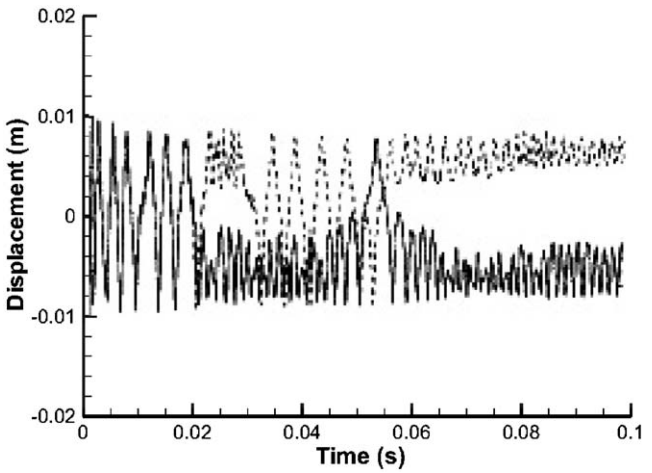

Fig. 12. Time histories of displacement of a lightly damped 2dof system, when $\zeta = 0.01$: ——, $P = 1200.000001$ N; – – –, $P = 1200.000002$ N [60].

It should be noted that the counterintuitive behavior described in Refs. [57–60] is not merely a computational phenomenon, nor is it limited to occurring only in beams. Li et al. [61], as well as Kolsky et al. [62], witnessed said behavior while experimentally testing clamped aluminum alloy beams impacted at mid-span. Varying the impact velocity instead of ϕ_0, the former authors observed the anomalous behavior about half the time when velocities ranged between 39 and 50 m/s. Moreover, amongst recent papers, Bassi et al. [63] documented the behavior in plates, Lepik [64] in cylindrical shells and Galiev [65] in both plates and shells.

Further, it is also worth noting that, as briefed in Refs. [63,65], the counterintuitive behavior was actually documented in the Soviet Union nearly a decade prior to Symonds and Yu [57]. The Soviet study found that, at times, circular metal plates displaced opposite the load direction when subjected to an underwater explosive blast. Galiev [65] also cited a similar study performed in air. Clearly, this phenomena could easily occur due to an explosion on board an aircraft.

From this section, it is seen that:

- Care must be taken when transferring a loading model from paper to a computer program.
- Sensitivity of all parameters must be considered when validating results, particularly when a structure exhibits small plastic deformation.
- Counterintuitive behavior can be explained by analyzing energy relations and power density spectra.

8. Probabilistic loading models

To this point, only deterministic loading models, in terms of pulse and distribution shape, have been considered. But due to uncertainties inherent to an explosion, random models are more appropriate. In this section, studies using probabilistic models in conjunction with previously mentioned methods are discussed.

But before proceeding, some necessary probability is now briefly reviewed. A probability density function (PDF), $f_X(x)$, maps the relative likelihood of a particular value of a variable x occurring. The area under the $f_X(x)$ curve equals 1, denoting that x will always fall within a specified range of values. Common PDFs include the uniform, normal, lognormal and Poisson densities. The normal, or Gaussian, density is governed by

$$f_X(x) = \frac{1}{\sigma\sqrt{2\pi}} \exp\left[-\frac{1}{2}\left(\frac{x-\mu}{\sigma}\right)^2\right],$$

where μ is the mean and σ the standard deviation of variable x. Plotting $f_X(x)$ versus x for $-\infty < x < \infty$ yields the classic bell-shaped curve, which shows that a randomly selected x is most likely close to the mean, and almost always within three standard deviations of the mean. Many naturally occurring processes are governed by a Gaussian distribution.

Furthermore, a joint probability distribution, $f_{X_1X_2\ldots X_n}(x_1, x_2, \ldots, x_n)$, maps the relative likelihood of n events occurring simultaneously. However, a bomb explosion is a random process with respect to both space and time. Therefore, an appropriate density function would be of the form $f_{X_1X_2\ldots X_n}(x_1, x_2, \ldots, x_n; t_1, t_2, \ldots, t_n)$. But such a density function can be difficult to

deal with mathematically. As a simplification, a stationary process can be assumed, i.e.,

$$f_{X_1X_2\ldots X_n}(x_1, x_2, \ldots, x_n; t_1, t_2, \ldots, t_n) = f_{X_1X_2\ldots X_n}(x_1, x_2, \ldots, x_n; t_1 + \Delta t, t_2 + \Delta t, \ldots, t_n + \Delta t). \tag{24}$$

For a one- or two-event stationary process, respectively, Eq. (24) reduces to

$$f_X(x, t) = f_X(x) \tag{25}$$

and

$$f_{X_1X_2}(x_1, x_2; t_1, t_2) = f_{X_1X_2}(x_1, x_2; \tau), \tag{26}$$

where $\tau = t_2 - t_1$. Eq. (25) can be used to find the first-order probability moment, or mean, of a stationary process. Likewise, Eq. (26) can be used to find second-order moments, such as the autocorrelation function $R_{XX}(\tau)$ or cross-correlation function $R_{XY}(\tau)$, which are simply a measure of randomness. It is common that a nonstationary process, such as an earthquake or bomb explosion, be modeled as the product of a stationary function and a deterministic envelope.

When $\tau = 0$, the autocorrelation function reduces to the mean square value of the variable $X(t)$, or $\mathbf{E}\{X(t)^2\}$, which, depending on the physical definition of $X(t)$, can be a measure of a process' average energy. The power spectral density (PSD) function, $S(\omega)$, is simply the Fourier transform of $R_{XX}(\tau)$. As such, it too is a measure of the energy distribution of a process, but in the frequency domain as opposed to the time domain. Similarly, the cross-power spectral density (CSD) is defined as the Fourier transform of $R_{XY}(\tau)$.

A typical PSD function, as shown in Fig. 13(a), will only have a large peak at one or a few select frequencies. These are the key frequencies to focus upon when using a modal approximation technique [10,11] for determination of maximum structural deflection. In contrast, a white noise process, shown in Fig. 13(b), is a mathematical idealization that assumes $S(\omega)$ is constant for all ω. Many studies assume such a PSD function. Ref. [66] can be consulted for a much more detailed discussion on the presented probability topics.

Kennedy and Iyengar [67] considered a pin-ended, viscoplastic, or strain-rate sensitive, circular plate subjected to a transverse pulse load having a Gaussian distribution. They used a simplified yield condition which considered bending moments and membrane forces separately. Despite this simplification, trials were made both including and excluding membrane force interaction in the moment-dominant deformation phase I. In contrast, phase II only accounted for membrane

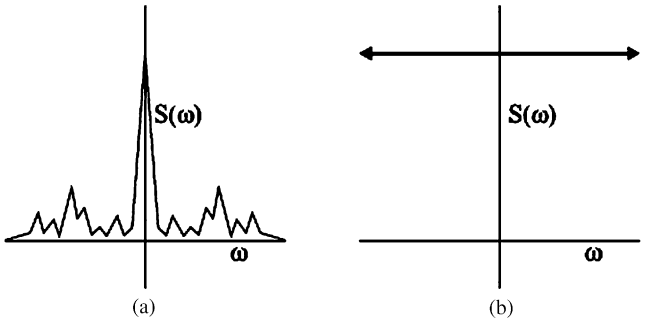

Fig. 13. Representative PSD functions: (a) general PSD; (b) white noise process.

force effects. In all cases though, plate deflections were dependent on a parameter g given as

$$g = \frac{b}{\sigma\sqrt{2}},$$

where b is the radius of the plate, and σ the standard deviation of the loading. By changing g, any loading ranging from a uniform distribution ($g \to 0$) to a concentrated force ($g \to \infty$) could be simulated. Comparing these two extreme cases for varying strain-rate sensitivities, the authors found that for large impulses, calculations that excluded membrane forces in phase I always overestimated maximum deflection. However, for smaller impulses, ignoring membrane forces underestimated maximum deflection at higher values of g. For both small and large impulses, a viscoplastic plate yielded only slightly higher deflections than its strain-rate insensitive counterpart. For equal impulses, plates with $g = 2.5$ centrally deflected about five times as much as those with $g = 0.05$. Therefore, the pulse shape effect plays a significant role even when a loading is probabilistically determined.

Chang [68] subjected a simple space structure model to a random excitation, $p(x, t)$. The model consisted of a hysteretically damped, free–free beam with a concentrated mass M variably located a distance a from one of the ends. The beam deflection, $y(x, t)$, depended on the following equation of motion:

$$EI(1 + \mathrm{i}\zeta)\frac{\partial^4 y(x,t)}{\partial x^4} + [m + M\delta(x-a)]\frac{\partial^2 y(x,t)}{\partial t^2} = p(x,t),$$

where E is Young's modulus, I the area moment of inertia of the beam, m the beam's mass per unit length, and ζ the hysteretic damping ratio. Assuming $p(x, t)$ stationary and the cross-correlation function, $R_{p_{x_1}p_{x_2}}$, known, modal techniques were used to find the loading's cross-spectral density CSD function and, in turn, the mean square values of displacement, bending moment, stress and strain along the beam. For example, the mean square displacement was given by

$$\mathbf{E}[y^2(x)] = \frac{1}{2\pi}\sum_{j=1}^{\infty}\sum_{k=1}^{\infty}\phi_j(x)\phi_k(x)\int_{-\infty}^{+\infty} H_j(\omega)H_k^*(\omega)S_{Q_jQ_k}(\omega)\,\mathrm{d}\omega,$$

where $\phi_j(x)$ represents the mode shape of the jth mode, ω is the frequency, and $S_{Q_jQ_k}(\omega)$ is the modal forcing's CSD function. Meanwhile, $H_j(\omega)$ is the frequency response function defined by

$$H_j(\omega) = \frac{1}{(1 + \mathrm{i}\zeta)\omega_j^2 - \omega^2},$$

where ω_j is the natural frequency of the jth mode, and $H_j^*(\omega)$ is a complex conjugate. Assuming a CSD function of the form $S_0\mathrm{e}^{-\alpha(x_1-x_2)}\mathrm{e}^{-\beta\omega^2}$, where α and β are constants, Chang found that increasing S_0 increased the uncertainty of the loading. This, in turn, increased the structure's probability of failure. Unfortunately, the techniques used were valid only for linear systems. Therefore, only elastic systems subjected to forces well below those that would cause yielding can be dealt with in a like manner. Yet, some extension can still be made to elastic–plastic structures, particularly free–free beams.

Dolinski [69] formally defined the failure condition for a rigid plastic structure under random loading in terms of its motion, $\mathbf{x}$, with respect to a linear limit surface, $S_L(\mathbf{x}) = 0$. Assuming that the

load vector, $\mathbf{X}(t)$, was a Gaussian process with stationary, twice differentiable components, he stated that the plastic deformation, $\mathbf{U}(t)$, could be represented as the summation of a random number of incremental displacements. These incremental values were only functions of the following five parameters: τ^f, the duration of structural motion, $\mathbf{X}(t^0)$ and $\mathbf{X}(t')$, the loads at which $\mathbf{x}$ leaves and returns to the limit surface, respectively, and $\mathbf{X}^{oE}$ and $\mathbf{X}'^{E}$, the respective equivalent levels of $\mathbf{X}(t)$ during and after excursion from the limit surface. The last two parameters were given by

$$\mathbf{X}^{oE} = \frac{1}{t' - t^0} \int_{t^0}^{t'} \mathbf{X}(\tau)\, \mathrm{d}\tau$$

and

$$\mathbf{X}'^{E} = \frac{1}{t^f - t'} \int_{t'}^{t^f} \mathbf{X}(\tau)\, \mathrm{d}\tau,$$

where t^f is the time when motion stops. These equivalent loads are reminiscent of the effective load defined in Eq. (9). In order to determine the actual magnitude of each incremental plastic displacement and therefore of $\mathbf{U}(t)$, Dolinski transformed all $\mathbf{X}$ values into Taylor expansions of $\mathbf{x}(t)$. This transformation allowed him to apply a standard modal approximation technique, like that of Eq. (3), to calculate $\mathbf{U}(t)$. The aforementioned assumptions enabled the displacement vector to be modeled as a Markov process, one whose future probabilities are determined by its most recent values, and the structural reliability, $R(t)$, to be governed by a Poisson distribution.

Li and Liu [70] accounted for uncertainty in their analytic treatment of the counterintuitive phenomenon of Symonds and Yu [57]. They used the pin-ended, elastic–plastic beam model of the previous authors, and subjected it to a rectangular pulse with a normally distributed pressure intensity, p_0. This pulse's mean intensity of 0.9465 MPa was equal to the mean of the calculated range of counterintuitive occurrence, $0.903 \leqslant p_0 \leqslant 0.990$ MPa. A standard deviation of 5% of the range width was assumed. Randomly selecting 180 values of p_0 with the given distribution, the anomalous response was recorded 58% of the time. This percentage was similar to the experimentally observed 50% of Li et al. [61]. Therefore, uncertainty of parameters should be introduced when modeling a parameter sensitive system, such as the pin-ended beam, to more closely capture its actual physical behavior.

From this section, it is seen that:

- In order to work with complicated probabilistic data, often times, simplications must be made. Two such simplications are a stationary and white noise process.
- Some techniques previously discussed for deterministic loads can be extended for use with random loads.
- Random loads are more realistic than purely deterministic loading models. They can capture actual physical phenomena, which may seem counterintuitive otherwise.

9. Concluding remarks

This review summarizes studies carried out throughout the last fifty years which can be applied to modeling a bomb explosion on an aircraft. Beams, plates, shells and sdof systems are used as representative structures subjected to variously shaped pulse pressure loads. Altering attributes

of the loading model, such as impulse, peak pressure, rise time and pulse duration, is shown to have a significant effect on maximum deformation sustained by these structures. Youngdahl, in particular, developed methods to essentially eliminate this effect in the four considered structures, assuming rigid plastic behavior. The applicability of these methods to random loads on elastic–plastic structures must be tested.

Furthermore, the behavior of free–free beams is closely examined. Such beams can absorb large amounts of energy from an explosive load, much of which goes into rigid body motion. This transfer of energy must be dealt with in an actual aircraft.

Moreover, the sensitivity of response to loading model, as well as to all material parameters, must be thoroughly investigated. Without doing so, the validity of all results is questionable. The use of a probabilistic loading model can only compound this uncertainty. However, pressure–impulse isodamage curves, shown to be an effective means of testing the damage-sustaining capability of a structure subjected to a deterministic loading, can easily be extended to cases involving a more random loading.

Acknowledgements

The authors thank the Transportation Security Administration (DHS) for their financial support of this review. In particular, they thank Howard Fleisher of the Transportation Security Laboratory and Abdelfattah Zebib of Rutgers University for their assistance throughout the duration of the former author's fellowship.

References

[1] K.P.R. Smart, The Lockerbie investigation: understanding of the effects of the detonation of 'improvised explosive devices' on aircraft pressure cabins, *IChemE Process Safety and Environmental Protection* 75 (1997) 138–144.
[2] J.A. Gatto, S. Krznaric, Pressure loading on a luggage container due to an internal explosion, in: Y.S. Shin, J.A. Zukas (Eds.), *Structures Under Extreme Loading Conditions-1996*, ASME, New York, NY, 1996, pp. 29–35.
[3] V.L. Chen, First successful simulation of on-board explosion will aid in aircraft hardening studies, *Simulation* 68 (1997) 107–110.
[4] D. Dietz, FEA makes airframes safer, *Mechanical Engineering* 120 (1998) 64–65.
[5] J.M. Biggs, *Introduction to Structural Dynamics*, McGraw-Hill, Inc., New York, NY, 1964.
[6] N. Jones, *Structural Impact*, Cambridge University Press, Cambridge, UK, 1989.
[7] H.J. Fleisher, Design and explosive testing of a blast resistant luggage container, in: N. Jones, C.A. Brebbia, A.J. Watson (Eds.), *Structures Under Shock and Impact IV*, Computational Mechanics, Inc., Billerica, MA, 1996, pp. 51–60.
[8] S.K. Singh, V.P. Singh, Mathematical modelling of damage to aircraft skin panels subjected to blast loading, *Defence Science Journal* 41 (1991) 305–316.
[9] S. Kaliszky, *Plasticity: Theory and Engineering Applications*, Elsevier Science Publishers, Amsterdam, The Netherlands, 1989.
[10] P.S. Symonds, A review of elementary approximation techniques for plastic deformation of pulse-loaded structures, in: S.R. Reid (Ed.), *Metal Forming and Impact Mechanics*, Pergamon Press, Ltd., Oxford, UK, 1985, pp. 175–194.
[11] J.B. Martin, P.S. Symonds, Mode approximations for impulsively-loaded rigid-plastic structures, *ASCE Journal of the Engineering Mechanics Division* 92 (EM5) (1966) 43–66.

[12] G.K. Schleyer, S.S. Hsu, A modelling scheme for predicting the response of elastic–plastic structures to pulse pressure loading, *International Journal of Impact Engineering* 24 (2000) 759–777.
[13] N. Jones, A literature review of the dynamic plastic response of structures, *Shock and Vibration Digest* 7 (8) (1975) 89–105.
[14] N. Jones, Recent progress in the dynamic plastic behavior of structures, part I, *Shock and Vibration Digest* 10 (9) (1978) 21–33.
[15] N. Jones, Recent progress in the dynamic plastic behavior of structures, part III, *Shock and Vibration Digest* 13 (10) (1981) 3–16.
[16] N. Jones, Recent progress in the dynamic plastic behaviour of structures, part IV, *Shock and Vibration Digest* 17 (2) (1985) 35–47.
[17] N. Jones, Recent progress in the dynamic plastic behavior of structures, part V, *Shock and Vibration Digest* 21 (8) (1989) 3–13.
[18] N. Jones, Recent studies on the dynamic plastic behavior of structures, *Applied Mechanics Review* 42 (1989) 95–115.
[19] N. Jones, Recent progress in the dynamic plastic behavior of structures, part VI, *Shock and Vibration Digest* 24 (11) (1992) 3–16.
[20] N. Jones, Recent studies on the dynamic plastic behavior of structures—an update, *Applied Mechanics Review* 49 (1996) S112–S117.
[21] W.J. Stronge, T.X. Yu, *Dynamic Models for Structural Plasticity*, Springer-Verlag, London, UK, 1993.
[22] P.D. Smith, J.G. Hetherington, *Blast and Ballistic Loading of Structures*, Butterworth-Heinemann Ltd., Oxford, UK, 1994.
[23] P.G. Hodge Jr., The influence of blast characteristics on the final deformation of circular cylindrical shells, *ASME Journal of Applied Mechanics* 23 (1956) 617–624.
[24] R.S. Ayre, Transient response to step and pulse functions, in: C.M. Harris (Ed.), *Shock and Vibration Handbook*, McGraw-Hill, Inc., New York, NY, 1961, pp. 8-1–8-54 (Chapter 8).
[25] W.J. Stronge, Efficient pulse shapes to plastically deform beams, *ASME Journal of Applied Mechanics* 41 (1974) 604–608.
[26] W.J. Stronge, Lower bound on deformation for dynamically loaded rigid-plastic structures, *International Journal of Solids and Structures* 19 (1983) 1049–1063.
[27] D.N. Robinson, A displacement bound principle for elastic–plastic structures subjected to blast loading, *Journal of Mechanics and Physics of Solids* 18 (1970) 65–80.
[28] P.S. Symonds, C.W.G. Frye, On the relation between rigid-plastic and elastic–plastic predictions of response to pulse loading, *International Journal of Impact Engineering* 7 (1988) 139–149.
[29] Ch. Zhang, D. Gross, Pulse shape effects on the dynamic stress intensity factor, in: *On Wave Propagation in Elastic Solids with Cracks*, Computational Mechanics Publications, Southampton, UK, 1998, pp. 45–59 (Chapter 3).
[30] R.B. Schubak, D.L. Anderson, M.D. Olson, Simplified dynamic analysis of rigid-plastic beams, *International Journal of Impact Engineering* 8 (1989) 27–42.
[31] D.Z. Yankelevsky, Y.S. Karinski, Dynamic elasto-plastic response of symmetrically loaded beams, *Computers and Structures* 76 (2000) 445–459.
[32] E.H. Lee, P.S. Symonds, Large plastic deformations of beams under transverse impact, *ASME Journal of Applied Mechanics* 19 (1952) 308–314.
[33] P.S. Symonds, Dynamic load characteristics in plastic bending of beams, *ASME Journal of Applied Mechanics* 20 (1953) 475–481.
[34] N. Jones, T. Wierzbicki, Dynamic plastic failure of a free–free beam, *International Journal of Impact Engineering* 6 (1987) 225–240.
[35] T.X. Yu, J.L. Yang, S.R. Reid, C.D. Austin, Dynamic behaviour of elastic–plastic free–free beams subjected to impulsive loading, *International Journal of Solids and Structures* 33 (1996) 2659–2680.
[36] J.L. Yang, F. Xi, Experimental and theoretical study of free–free beam subjected to impact at any cross-section along its span, *International Journal of Impact Engineering* 28 (2003) 761–781.
[37] J.L. Yang, T.X. Yu, S.R. Reid, Dynamic behaviour of a rigid, perfectly plastic free–free beam subjected to step-loading at any cross-section along its span, *International Journal of Impact Engineering* 21 (1998) 165–175.

[38] T.U. Ahmed, L.S. Ramachandra, S.K. Bhattacharyya, Elasto-plastic response of free–free beams subjected to impact loads, *International Journal of Impact Engineering* 25 (2001) 661–681.
[39] Y. Zhang, J.L. Yang, Dynamic plastic behaviour of a notched free–free beam subjected to step-loading at one end, *International Journal of Pressure Vessels and Piping* 79 (2002) 741–752.
[40] H.H. Ruan, T.X. Yu, Deformation mechanism and defect sensitivity of notched free–free beam and cantilever beam under impact, *International Journal of Impact Engineering* 28 (2003) 33–63.
[41] C.K. Youngdahl, Correlation parameters for eliminating the effect of pulse shape on dynamic plastic deformation, *ASME Journal of Applied Mechanics* 37 (1970) 744–752.
[42] C.K. Youngdahl, Dynamic plastic deformation of circular cylindrical shells, *ASME Journal of Applied Mechanics* 39 (1972) 746–750.
[43] C.K. Youngdahl, Dynamic plastic deformation of a tube loaded over a time-dependent region, *International Journal of Impact Engineering* 9 (1990) 71–88.
[44] C.K. Youngdahl, D. Krajcinovic, Dynamic plastic deformation of an infinite plate, *International Journal of Solids and Structures* 22 (1986) 859–881.
[45] C.K. Youngdahl, Influence of pulse shape on the final plastic deformation of a circular plate, *International Journal of Solids and Structures* 7 (1971) 1127–1142.
[46] C.K. Youngdahl, Effect of pulse shape and distribution on the plastic deformation of a circular plate, *International Journal of Solids and Structures* 23 (1987) 1179–1189.
[47] C.K. Youngdahl, The interaction between pulse shape and strain hardening in dynamic plastic response, *International Journal of Impact Engineering* 7 (1988) 55–70.
[48] G.R. Abrahamson, H.E. Lindberg, Peak load-impulse characterization of critical pulse loads in structural dynamic, *Nuclear Engineering and Design* 37 (1976) 35–46.
[49] G. Zhu, Y.-G. Huang, T.X. Yu, R. Wang, Estimation of the plastic structural response under impact, *International Journal of Impact Engineering* 4 (1986) 271–282.
[50] R. Vaziri, M.D. Olson, D.L. Anderson, Dynamic response of axially constrained plastic beams to blast loads, *International Journal of Solids and Structures* 23 (1987) 153–174.
[51] Q.M. Li, H. Meng, Pressure–impulse diagram for blast loads based on dimensional analysis and single-degree-of-freedom model, *Journal of Engineering Mechanics* 128 (2002) 87–92.
[52] Q.M. Li, H. Meng, Pulse loading shape effects on pressure–impulse diagram of an elastic–elastic, single-degree-of-freedom structural model, *International Journal of Mechanical Sciences* 44 (2002) 1985–1998.
[53] Q.M. Li, N. Jones, Blast loading of fully clamped circular plates with transverse shear effects, *International Journal of Solids and Structures* 31 (1994) 1861–1876.
[54] Q.M. Li, N. Jones, Blast loading of a ''short'' cylindrical shell with transverse shear effects, *International Journal of Impact Engineering* 16 (1995) 331–353.
[55] Q.M. Li, N. Jones, Blast loading of fully clamped beams with transverse shear effects, *Mechanics of Structures and Machines* 23 (1995) 59–86.
[56] J.M. Santiago, S. Bhattacharya, Sensitivity of plate response calculations to blast load definition, *Computers and Structures* 40 (1991) 375–392.
[57] P.S. Symonds, T.X. Yu, Counterintuitive behavior in a problem of elastic–plastic beam dynamics, *ASME Journal of Applied Mechanics* 52 (1985) 517–522.
[58] G. Borino, U. Perego, P.S. Symonds, An energy approach to anomalous damped elastic–plastic response to short pulse loading, *ASME Journal of Applied Mechanics* 50 (1989) 430–438.
[59] J.-Y. Lee, P.S. Symonds, G. Borino, Chaotic responses of a two-degree-of-freedom elastic–plastic beam model to short pulse loading, *ASME Journal of Applied Mechanics* 59 (1992) 711–721.
[60] Y. Qian, P.S. Symonds, Anomalous dynamic elastic–plastic response of a Galerkin beam mode, *International Journal of Mechanical Sciences* 38 (1996) 687–708.
[61] Q.M. Li, L.M. Zhao, G.T. Yang, Experimental results on the counterintuitive behaviour of thin clamped beams subjected to projectile impacts, *International Journal of Impact Engineering* 11 (1991) 341–348.
[62] H. Kolsky, P. Rush, P.S. Symonds, Some experimental observations of anomalous response of fully clamped beams, *International Journal of Impact Engineering* 11 (1991) 445–456.

[63] A. Bassi, F. Genna, P.S. Symonds, Anomalous elastic–plastic responses to short pulse loading of circular plates, *International Journal of Impact Engineering* 28 (2002) 65–91.
[64] U. Lepik, Axisymmetric vibrations of elastic–plastic cylindrical shells by Galerkin's method, *International Journal of Impact Engineering* 18 (1996) 489–504.
[65] S.U. Galiev, Distinctive features of counter-intuitive behavior of plates and shells after removal of impulse load, *International Journal of Impact Engineering* 19 (1997) 175–187.
[66] H. Benaroya, S.M. Han, *Probabilistic Models*, Textbook Manuscript, CRC Press, Boca Raton, FL, 2005, to be published.
[67] J.B. Kennedy, K.J. Iyengar, Behavior of viscoplastic circular plates under Gaussian impulse, *Nuclear Engineering and Design* 64 (1981) 117–128.
[68] T.-P. Chang, Dynamic response of space structures under random excitation, *Computers and Structures* 48 (1993) 575–582.
[69] K. Dolinski, Reliability of rigid-plastic structures under stochastic dynamic loading, in: A. Sawczuk, G. Bianchi (Eds.), *Plasticity Today: Modelling, Methods and Applications*, Elsevier Applied Science Publishers, Ltd., London, UK, 1985, pp. 361–374.
[70] Q.M. Li, Y.M. Liu, Uncertain dynamic response of a deterministic elastic–plastic beam, *International Journal of Impact Engineering* 28 (2003) 643–651.